This article has been accepted for publication in a future issue of this journal, but has not been fully edited. Content may change prior to final publication. Citation information: DOI 10.1109/TIA.2020.2966458, IEEE Transactions on Industry Applications

Low-Cost Interior Permanent Magnet Machine with Multiple Magnet Types

Qingqing Ma, *Member*, IEEE, Ayman EL-Refaie, *Fellow*, IEEE, Bruno Lequesne, *Fellow*, IEEE

***Abstract*— This paper is a contribution to answering the following question: Is it possible to design a permanent-magnet machine with the performance expected from rare-earth magnets, but at a lower cost? Performance being understood as torque, size, efficiency, demagnetization and temperature rise together. The question is addressed with a systematic exploration of different interior permanent-magnet machine topologies mixing rare-earth and ferrite permanent magnets. The study starts from a production baseline, the Prius 2010 traction motor, with interior magnets placed in a single V pattern. It investigates various rotor designs, most specifically, single V and double V patterns as well as spoke configurations. The stator cross-section design and winding selection are fixed, providing a solid comparison basis from the point of view of machine cooling. For each rotor design, torque potential and machine material cost are assessed, the latter expressed as torque per dollar. A promising configuration was found, based on a spoke pattern, for which further modeling was performed to assess efficiency as well as mechanical strength and resistance to short circuits and to demagnetization. It reduces the rare earth magnet volume by over 60%.**

***Index Terms*—Finite elements analysis (FEA), interior permanent magnet machine, rare earth, ferrite, cost, magnetostatics**

I. INTRODUCTION

INTERIOR permanent magnet (IPM) synchronous machines are leading candidates for a number of applications such as industrial, renewable energy and vehicle traction, due to their higher power density and efficiency. However, cost and supply-chain concerns for rare-earth magnets present challenges which are absent in induction, synchronous-reluctance and switched-reluctance machines. Much effort has thus been dedicated to developing machine designs with performance on par with that of IPM machines with rare earth, but at a lower cost. The proposed paper focuses on solutions based on low-cost magnets such as ferrite.

Machines with ferrite magnets existed before rare-earth magnets were invented, and their design was revisited recently to take advantage of advances in IPM machine design [1-9]. Some place the magnets in one [3], two [8] or multiple [2,5,6] V patterns, the latter being perhaps better characterized as magnet-enhanced synchronous reluctance machines. Others place the magnets like spokes in a wheel [4,6,7-9], thus concentrating the magnet flux towards the airgap. Either way, when a direct comparison is made with a rare-earth based equivalent, the numbers vary but the conclusions are similar: With ferrite only, a match in performance with rare-earth has not proven possible to date. For instance, in [3], the ferrite motor (with a single V pattern) is 24% to 53% heavier (active mass) than a motor with neodymium-based magnets (24% if the rare earth contains no heavy rare-earth, 53% when it does). In [2], a ferrite IPM is compared with a surface PM (rare-earth) motor. The ferrite design is cheaper, but the stack length is 15% longer. In [7], for an air conditioner application, the motor size and output are similar, but the configuration with rare-earth magnets is a near-surface (not V-shaped IPM) design. Interior PM designs have significant reluctance torque, thus enjoying better torque density. Only one efficiency point is shown, with the ferrite motor peaking at 90.0% while the rare-earth motor peaks at 91.9%, an almost 2 percentage-point difference. The study in [4] is specifically for automotive traction. The ferrite-based machine is 31% heavier and the efficiency at 2800 rpm is 0.2 to 1.5 percentage points less than with a comparable rare-earth motor. In [9], for a starter-generator, a ferrite spoke motor provides 30% less specific torque than a Neodymium-based motor (with a V pattern), with both designs having undergone a large-scale optimization process. Considering that the energy product of ferrite magnets is 10 times smaller than that of neodymium magnets, these results are noteworthy, but not sufficient for demanding applications such as traction.

Accordingly, a number of authors are looking at more complex and sometimes radically new motor topologies such as Vernier machines [10], flux switching machines [11,12], or internally geared machines [13]. In this paper, we focus on a different approach, namely blending different magnet types, specifically ferrite and neodymium-based materials. This has been attempted before. In [14], a novel rotor configuration is proposed, which comprises two axially-separated rotors with conventional, buried rare-earth magnets, and a claw-pole structure in-between to add flux from a ferrite disk magnet. The torque and efficiency are higher than with conventional IPM machines, but the proposed rotor structure is complex, with associated manufacturing and mechanical concerns. Also, no cost comparison is presented. Ref. [15] provides an interesting treatise of magnet placement and reluctance optimization in the blended magnet type, and points to demagnetization of the

The manuscript was received on Aug.28 2019.

Qingqing Ma is with the Department of Electrical and Computer Engineering, Marquette University, Milwaukee, WI, 53233 USA (e-mail: qingqing.ma@marquette.edu).

Ayman EL-Refaie is with the Department of Electrical and Computer Engineering, Marquette University, Milwaukee, WI, 53233 USA (e-mail: ayman.el-refaie@marquette.edu).

Bruno Lequesne is with E-Motors Consulting LLC, Menomonee Falls, WI, 53051 USA (e-mail: bruno@emotorseng.com).

This article has been accepted for publication in a future issue of this journal, but has not been fully edited. Content may change prior to final publication. Citation information: DOI 10.1109/TIA.2020.2966458, IEEE Transactions on Industry Applications

weak magnet by the strong one as a manufacturing concern. It claims that the new design reaches a performance similar to that of a rare-earth-only motor. However, the comparison is made at one point only and the price advantage is stated but not substantiated. The authors in [16] propose a single layer V-type IPM design with ferrite and rare-earth magnets and compare the performance in terms of reluctance and reaction torques, and efficiency. Their design improves the cost by 19% (based on 2012 rare-earth prices) and increases torque by 4%. However, demagnetization studies are limited to short-circuit condition at common temperatures. Demagnetization at extremes (on the order of 140°C for Nd and -20°C for ferrite) is not investigated. We will see this as a critical issue for blended-magnet configurations.

This paper expands on the results of [16] by analyzing a variety of rotor topologies, broadly classified in two categories: V-shaped and spoke type, with various blends of ferrite and rare-earth magnets, varied in terms of layout as well as proportions. The performance is calculated in terms of torque density and performance per dollar among other metrics. This process is used to identify the most cost-effective design that significantly reduces the rare-earth content while maintaining the high performance of a rare-earth design. The paper also adds various additional studies to a conference paper, in particular mechanical stress calculations, a short-circuit study and an in-depth demagnetization analysis [17].

The study uses as a baseline the Prius 2010 motor with V-shaped Nd magnets ([18], Fig.1). Table I shows the key design parameters of that machine. Note that the actual machine (Fig. 1a) includes cavities in the rotor, which help with air flow and cooling and reduce weight and inertia. These were not included in the model (Fig.1b) which focused on electromagnetics.

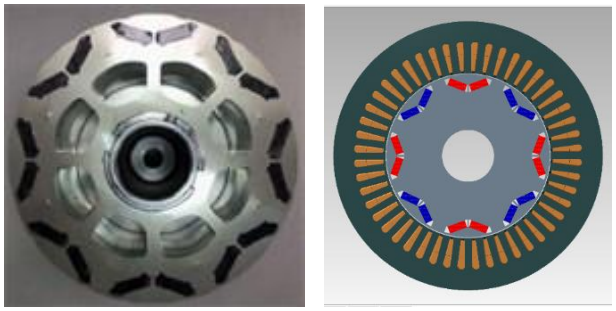

(a) Actual rotor (from [18], with permission) (b) Model

Fig. 1: Prius 2010 motor (baseline)

TABLE I
BASELINE DESIGN CHARACTERISTICS [18]

Dimensions (mm)	Prius 2010 motor
Stator outer diameter	264
Stator inner diameter	161.9
Rotor outer diameter	160.4
Rotor inner diameter)	51
Active stack length	50
Air gap length	0.73

During the study, the stator cross-section, winding configuration, air gap, rotor outer and inner diameters are the same as for the baseline. This approach makes it possible to keep the same basis for current density and machine cooling capacity. The thickness of the rotor's magnet bridges is also kept the same. This is therefore an initial design aimed at determining if the approach, i.e. having two magnet types, can provide similar torque at a lower cost. If the answer is yes, then subsequent work will include an overall optimization where some of these design parameters are allowed to vary, such as the stator design for instance. At the same time, these constraints in the analysis give an advantage to the baseline with NdFeB magnets, which was fully optimized. Accordingly, the present results are conservative, and, if a topology is found which is cheaper yet as performant without changing the stator or the magnet bridges, then further cost reductions or performance improvements can be expected from an optimization process (see Section III-F).

Some exemplary rotor configurations analyzed in the paper are shown in Figs. 2 and 3. In the figures, darker purple in the rotor denotes ferrite and grey NdFeB magnets (with a lighter purple for the iron). Referring to Fig. 2 (double-V shape), some configurations have one V composed of ferrite and the other of rare earth (Fig. 2a, called 2-V1), while others have both magnet types in the inner V as well as the outer V (Fig. 2b, denoted 2-V2). Figs. 3a and 3b show the proposed blended spoke IPM machine. The Nd magnets, again in grey, are near the surface and much smaller than the ferrite magnet (deeper in the rotor, dark purple). In Fig. 3a, the rare-earth magnet is shorter (along the azimuthal direction) than the ferrite magnet, while in Fig. 3b, they are of the same length.

Obviously, the total magnet volume is larger when one uses ferrite, but the goal is that the overall cost will be less. This, however, needs to be established by careful consideration of the material cost multiplied by the material requirement for each design, a process proposed in the paper to generalize the conclusions and establish when, in terms of material cost, one topology is better than another.

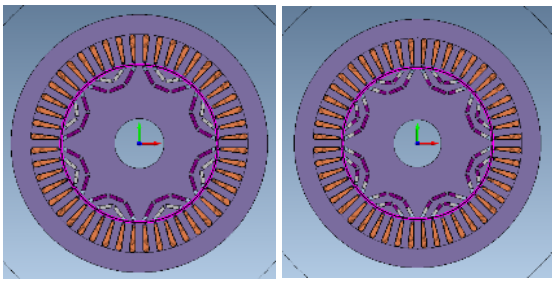

(a) Blended 2-V1 model (b) Blended 2-V2 model

Fig. 2: Blended magnets, V-shaped IPM (Nd in grey, ferrite in purple)

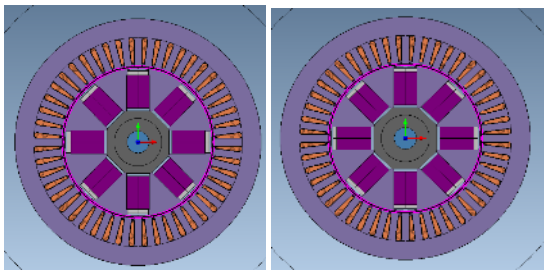

(a) Spoke, Nd shorter than ferrite (b) Spoke, ferrite and Nd equal length

Fig. 3: Blended magnets, spoke IPM (Nd in grey, ferrite in purple)

This article has been accepted for publication in a future issue of this journal, but has not been fully edited. Content may change prior to final publication. Citation information: DOI 10.1109/TIA.2020.2966458, IEEE Transactions on Industry Applications

II. Performance Comparison of Proposed Topologies

The proposed designs with different rotor topologies were modelled using 2D finite-element analysis (FEA) (MagNet software from Mentor Graphics). The analysis followed the "maximum torque per Ampere" (MTPA) operation trajectory. The magnet materials selected for the study were TDK FB13B for the ferrite, and for the rare earth magnets, Neodymium 45/15 (as provided by MagNet) in general, with several grade variants for the demagnetization analysis (material characteristics from [19]). The proposed V-shape magnet topologies were derived from the Prius, to which rare earth is substituted for ferrite at logical locations, most notably closer to the airgap where demagnetizing fields are strongest [15,16]. The spoke configuration, by contrast, is inspired primarily by ferrite designs, where the magnets' azimuthal flux is strongly amplified when it reaches the airgap by the relatively narrow steel passage between magnets [9]. The thought for those is to add some rare earth, enough to enhance the performance, not enough to compromise the price advantage.

Fig. 4 shows a sample of topologies that were analyzed. It illustrates the two basic approaches, V and spoke, as well as possible magnet placements (grey for ferrite, dark purple for NdFeB). The study included extremes, 100% ferrite and 100% NdFeB designs, to frame the results. Of note also is the placement of the magnets, sometimes in series (e.g., Fig. 4b), whereby the flux from one magnet type traverses the other magnet type, sometimes in parallel (Fig. 4c, as well as all the spoke designs), whereby the flux from the two magnet types merge as they flow towards the airgap. This aspect of the design, series versus parallel, is examined in details in [15] which concluded to the superiority of the parallel configuration. The present results are consistent with [15] in this regard.

For the spoke designs, bottom rows in Fig. 4, the NdFeB magnet length was varied relative to the ferrite magnet length. This is expressed in the captions with "L" denoting the ferrite magnet length and xL the Nd length. That is, 0.8L means the length of the NdFeB magnet is 80% of the ferrite length L, 1.0L same length, etc.

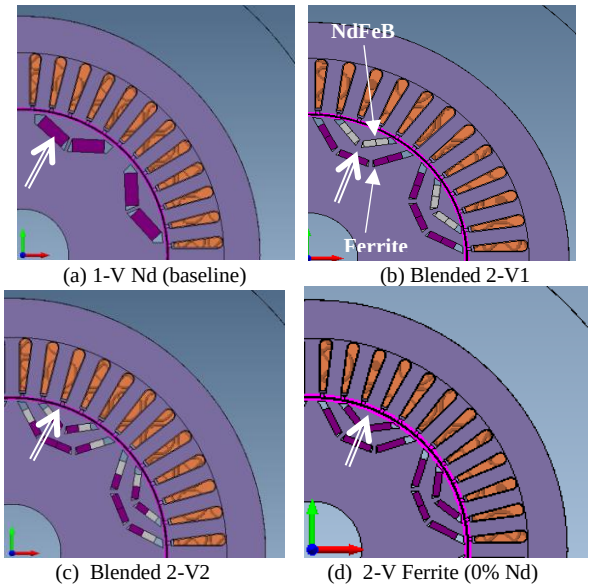

(a) 1-V Nd (baseline) (b) Blended 2-V1

(c) Blended 2-V2 (d) 2-V Ferrite (0% Nd)

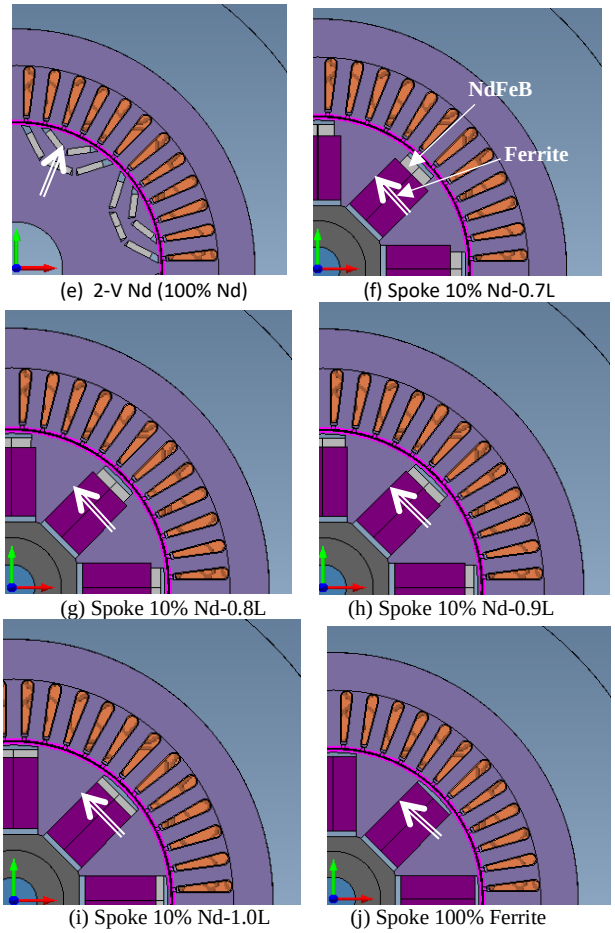

(e) 2-V Nd (100% Nd) (f) Spoke 10% Nd-0.7L

(g) Spoke 10% Nd-0.8L (h) Spoke 10% Nd-0.9L

(i) Spoke 10% Nd-1.0L (j) Spoke 100% Ferrite

Fig. 4: Proposed rotor configurations with different percentages of Nd magnet (Nd in grey, ferrite in dark purple, iron in light purple, magnetization direction shown by the thick white arrow).

A. *Torque performance*

Fig. 5 shows a comparison of the torque as a function of current angle under the 250A (peak) rated current operating condition. The torque shown is low speed torque (field weakening and high speed potential will be assessed later). It can be seen that several (though not all) spoke designs with various mixes of NdFeB and ferrites can produce comparable torque to the baseline design (slightly less). Every one of the two-layers, V-shaped designs considered here generates lower torque, most likely because the configuration does not lend itself to placing a large amount of ferrite.

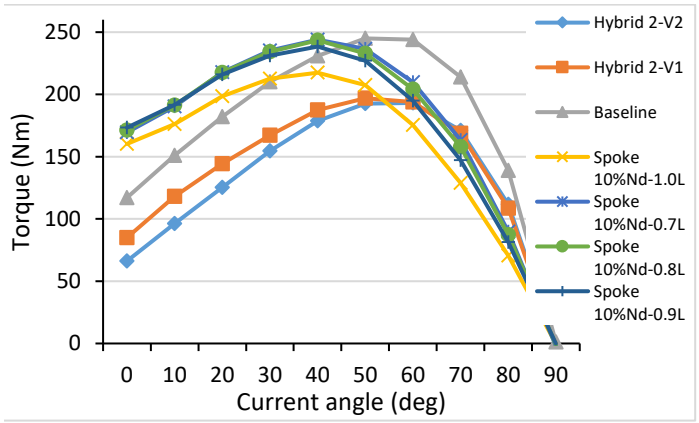

Fig. 5: Comparison of the output torque versus current angle

This article has been accepted for publication in a future issue of this journal, but has not been fully edited. Content may change prior to final publication. Citation information: DOI 10.1109/TIA.2020.2966458, IEEE Transactions on Industry Applications

Figs. 6 and 7 compare the magnet volumes and maximum torque generation for different rotor configurations (for the same stack length).

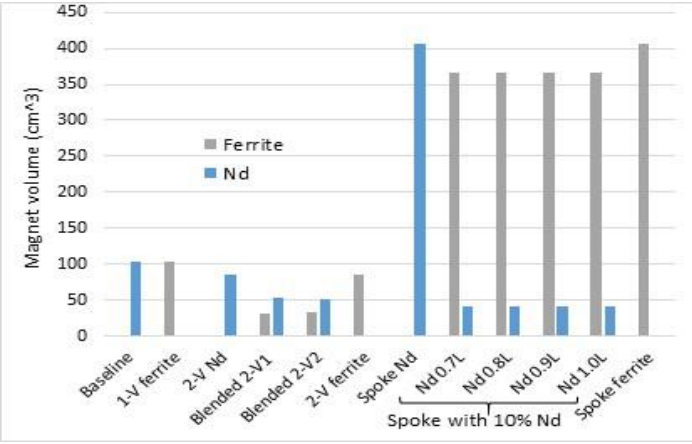

Fig. 6: Magnet volume for different configurations

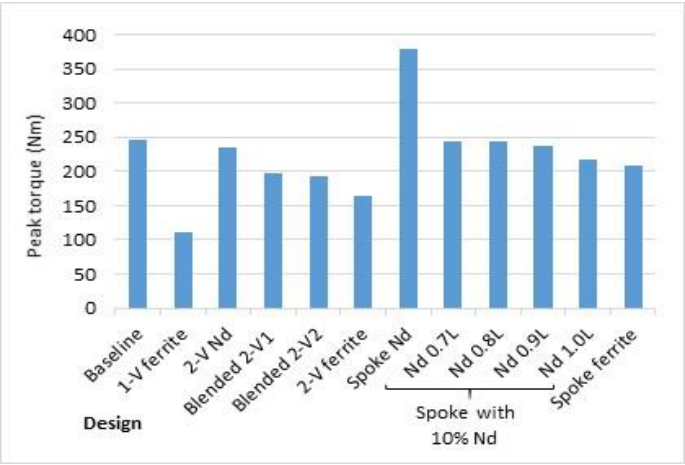

Fig. 7: Maximum torque at 1500 rpm for different configurations

The spoke designs with blended magnets can generate comparable torque, in several instances on par, with the baseline (245Nm, as calculated with MagNet for a machine with the Prius dimensions). The torque generation in spoke-type machines with unequal magnet lengths is larger than that of spoke-tye IPMs with equal magnet lengths when the exact same PM volume is used. This is likely because a shorter magnet is wider (for the same volume), thus generating more flux.

Another difference between spoke and V-shaped designs, not captured in the above, is the utilization of the rotor space. Spoke designs make full use of that space, having magnets extending all the way to the shaft. This can be considered an advantage. However, it comes with several drawbacks. With magnets placed only near the surface of the rotor, cavities can be punched in the rotor laminations (see Fig. 1, picture of actual Prius 2010 rotor), which reduces inertia and weight, and helps air flow, to some degree at least. Also, having magnetic rotor components near the shaft may make it necessary to use a non-magnetic material for the shaft, a possible cost increase.

B. Torque per dollar

Based on the analysis of torque performance, spoke designs with blended magnets can generate comparable torque to the baseline design with a much reduced rare-earth content but at the expense of a significant amount of ferrite. In order to evaluate the various designs from a material cost perspective, the produced torque per machine cost has to be investigated. We assumed an Nd price of $100/kg. This number is based on US Geological Survey data [20], showing a 2018 average of $51/kg for neodymium oxide, which must be augmented by additions (such as dysprosium, at $180/kg, etc), as well as some manufacturing cost for the final magnet. Ferrite prices often vary depending on grade. We used two numbers, $7/kg and $14/kg, to include a range of ferrite prices. Copper and lamination costs were assumed to be $7.03/kg and $1.0/kg, respectively [21].

The torque per dollar comparison is shown in Fig.8 for both assumptions concerning ferrite cost. The figure must be read as follows. Each bar represents a different design, described under the x-axis: From left to right, the baseline Prius, V-shaped designs, then spoke designs. The blue curve corresponds to the peak low-speed torque for each design, same data as in Fig. 7. The bars represent the torque per dollar for each design, or "Machine cost", calculated as follows:

$$Machine\ Cost = \left(V_{Nd} \times C_{Nd} + V_{fe} \times C_{fe} + V_{Cu} \times C_{Cu} + V_{lam} \times C_{lam}\right) \times L_{Machine}$$

Within the parentheses, V denotes the volume per unit length for each material, C is the material cost per volume, and the subscripts correspond to: Nd = rare-earth, fe = ferrite, Cu = copper and lam = laminations. The term in parentheses is multiplied by the length of the machine, $L_{Machine}$, calculated based on the ratio of the torque calculated for that particular design over the baseline torque, as follows:

$$L_{Machine} = \frac{T_{Machine}}{T_{Baseline}} \times L_{Baseline}$$

where $L_{baseline}$ is the length of the baseline machine, and $T_{machine}$ and $T_{baseline}$ are the torques for the calculated and baseline machines, respectively. In other words, the term in parentheses is the cost of the design per unit length, and the length of the machine is extended or reduced in proportion of the peak torque calculated for that design, relative to baseline, such that the resulting machine generates the same torque as baseline (it is well known that machine torque is proportional to rotor volume, or for a constant rotor diameter, to rotor length, at least as a first degree approximation). Looking for illustration at the bar to the right of the baseline (1V ferrite), this machine yields much less torque than baseline (blue curve), of course, since the Nd magnets are replaced by ferrite, but the torque per dollar (orange bar) is almost the same, because the machine must be much longer to provide the same torque.

It is important to note that cost calculations are based on active material cost only, excluding housing, shaft, bearings, etc. Most of the non-active parts of a spoke design are similar to those in a V-shape IPM, but with some exceptions. For instance, in order to avoid magnet flux leakage at the rotor core inner radius, a non-magnetic hub/shaft will be needed for the spoke design. Usually non-magnetic hubs/shafts are more expensive

This article has been accepted for publication in a future issue of this journal, but has not been fully edited. Content may change prior to final publication. Citation information: DOI 10.1109/TIA.2020.2966458, IEEE Transactions on Industry Applications

compared to magnetic hubs/shafts. For the motor size discussed, such differences might slightly alter the numbers but should not affect the overall conclusions.

Another element not included in this cost comparison is manufacturing cost. The blended magnet designs have advantages and disadvantages. Having two magnets per pole could be considered a manufacturing cost addition. However, several advantages mitigate this. First, ferrite is a much lower energy density magnet, therefore the cost of magnetizing and assembly should be less than for sintered NdFeB magnets. Second, ferrites have a much higher resistivity than sintered, rare-earth magnets, thus need not be segmented. As a result, the overall number of magnet pieces per machine may be smaller or at least not much higher. Magnet segmentation in the axial direction is often used in rare-earth, V-shape designs because the motors are usually high-frequency and some of them have fractional-slot concentrated windings, leading to rotor loss concerns. On balance therefore, combining two different magnets could actually result in further cost reduction from an assembly perspective.

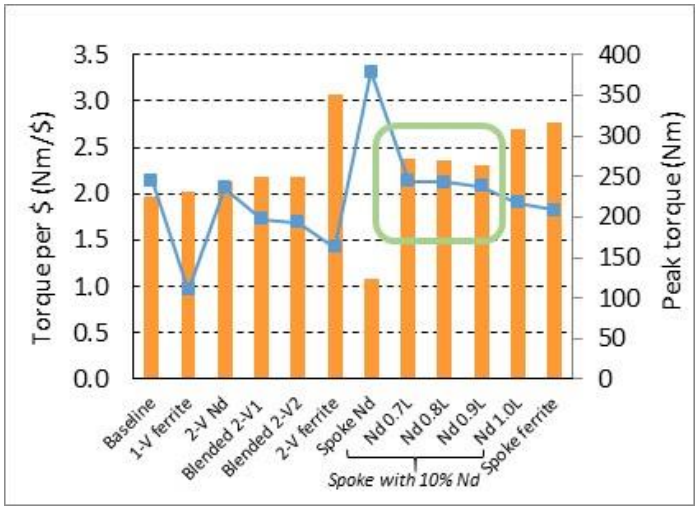

(a) Ferrite cost at $14/kg

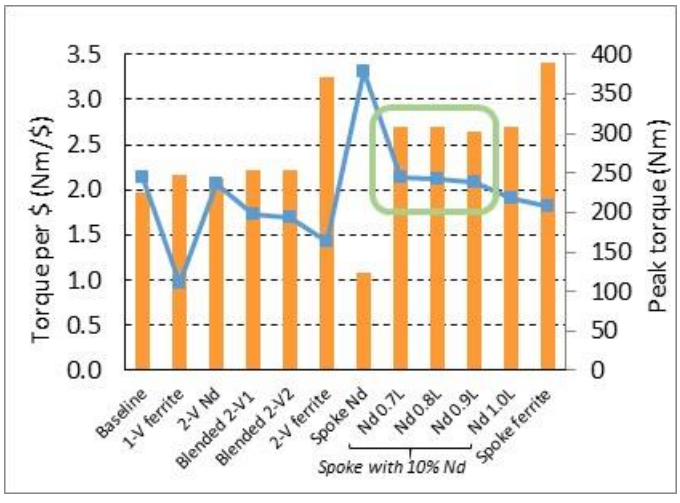

(b) Ferrite cost at $7/kg

Fig. 8: Comparison of torque per dollar for different rotor configurations
Bars: Torque per dollar; blue curve: Peak, low-speed torque

Looking at Fig. 8 overall, the best torque per dollar is obtained with all-ferrite designs, either a double V design or a spoke design. However, both of them produce some of the lowest torques, such that a much larger machine is needed for a given torque. They may be attractive options when space and weight are not a concern, but cost is.

In the remainder of the paper, however, we will focus on configurations which do not require a longer machine to get the same torque, as the objective of the study is to get performance at least on par with rare-earth based machines. In this regard, all blended V-shape and spoke-type IPM designs have an advantage over the baseline design in terms of torque/dollar. Among those, three designs (highlighted inside a green box on the figure) stand out in that they can generate as much torque (or marginally less torque) than baseline (see blue curves), with higher torques/dollar (orange bars). As seen by comparing Fig. 8a and Fig. 8b, the difference in torque per dollar between baseline design and blended-magnet, spoke type IPM is even larger if the cost of ferrite decreases since the spoke type IPM machine uses a large volume of ferrite material and much less Nd material. This is key and promising result from this study.

Fig. 8 does not show proportions of rare earth larger than 10%. Calculations, not included here for clarity, were performed with 20% and 30%, but cost increased more rapidly than torque. The opportunity, therefore, rests with a small amount of rare earth, on the order of 10%.

As illustrated in Fig. 8, the spoke design with 10% rare-earth magnets that are shorter than the ferrite (70%,) produces the same torque and is cheaper, even with the more expensive ($14/kg) of the two ferrite costs studied. This configuration was thus selected for further analysis.

The results in Fig. 8 are only a start in terms of price comparison, as raw material prices are not fixed in time. Susceptibility of the torque/dollar comparison to price variation is of importance. In other words, at what price point do these promising designs become less or more so? An answer is provided in Fig. 9: The price of neodymium is varied from $10/kg to $150/kg, assuming ferrite prices of either $7/kg (orange line) or $14/kg (green line). The price per dollar is then calculated for the Prius 2010 and the selected best of the blended spoke designs. There is a crossover around either $30/kg (for low-cost ferrite) or $55/kg (for higher-priced ferrite). Below these numbers, a machine is more cost-effective with Nd only (but there is still the sustainability concern of Nd magnets).

This article has been accepted for publication in a future issue of this journal, but has not been fully edited. Content may change prior to final publication. Citation information: DOI 10.1109/TIA.2020.2966458, IEEE Transactions on Industry Applications

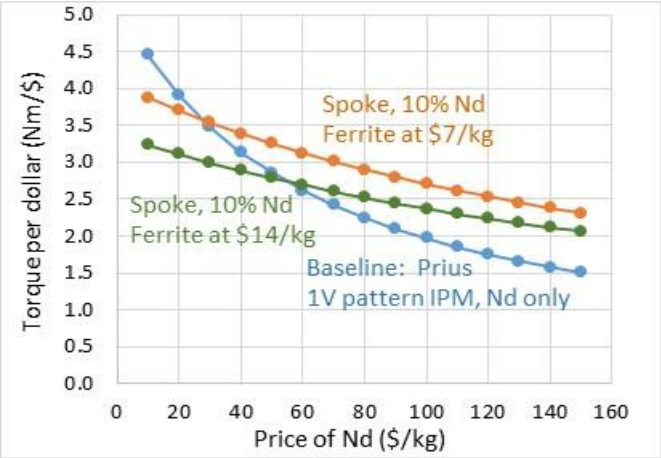

Fig. 9: Torque per dollar for the design with blended magnets compared to baseline, Prius 2010 with Nd only

These numbers, $30/kg to $55/kg, are not an absolute of course. First, they are a function of the cost of ferrite and, to a smaller degree, iron and copper. Also, designs with Nd only are improving, as engineers strive to use less magnet. Rare-earth magnet cost depends on heavy rare-earth content. Finally, the optimization of the blended configuration presented here requires more work, some of it presented below. Altogether, however, this shows first the importance of incorporating material pricing in the design of the machine, and careful weighing of both magnet grade properties and price expectation while designing. And second, the use of a blend of ferrite and Nd may well be cost-effective at current Nd prices, and is definitely so if these prices were to increase.

III. Design Consideration and Performance Evaluation

The selected design was further investigated in terms of speed range, efficiency, mechanical strength, short-circuit behavior, and demagnetization capability, concluding with possible optimization directions.

A. *Flux-weakening capability*

The focus so far was on low-speed torque, because it made for straightforward torque/dollar comparisons. Equally important for many applications such as traction is a wide speed range, which is a function to a large degree of flux weakening potential. The flux-weakening performance was evaluated based on a nonlinear model of the d-q flux linkage, by which the saturation effects can be taken into account. For a specific current, the maximum torque obtained is a combination of magnet torque and reluctance torque. The current angle γ_{MTPA} is defined as the current angle providing the MTPA.

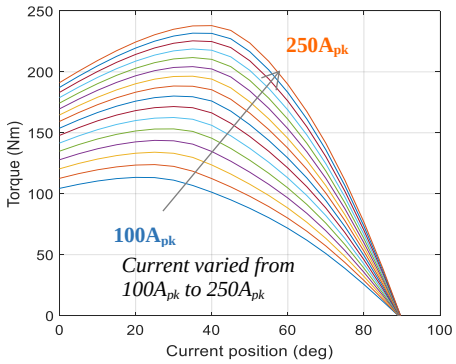

Fig. 10: Torque map versus current angle

Below base speed, the terminal voltage is not restrictive so the maximum nominal torque can be obtained for a constant current angle of γ_{MTPA}. Based on the nonlinear model of d-q flux linkage, a search algorithm for γ_{MTPA} by means of Matlab/M-file for optimizing the current angle was developed, by which the torque can be plotted under different current loading, as shown in Fig. 10 for 1500 rpm. The maximum dc-link voltage in the Prius 2010 is 650V [18]. The phase terminal voltage of the machine can be calculated by:

$$V_{max} = \frac{V_{dc-bus}*\sqrt{2}}{\pi} = 293\text{V}$$

With the assumption of maximum current 250A (peak) and DC bus voltage limit, the torque versus speed characteristic was derived in Fig. 11. The machine reaches the maximum voltage limit around 2800 rpm, below which the electrical machine runs at MTPA operation with the same current angle for a given current. Beyond 2800 rpm, the current angle has to increase to maintain sufficient armature current and allow the speed to increase. Fig. 11 compares the calculated results (without mechanical losses) to Prius FEA data obtained from MotorCAD software. The overall torque-speed curves are similar, including torque at maximum speed (ca. 37Nm) and speed at knee (ca. 2,800 rpm), indicating overall comparable performance. The slightly lower torque at low speed was mentioned already earlier. It appears therefore that the blending of magnet types does not impact (positively or negatively) the flux weakening potential of IPM machines.

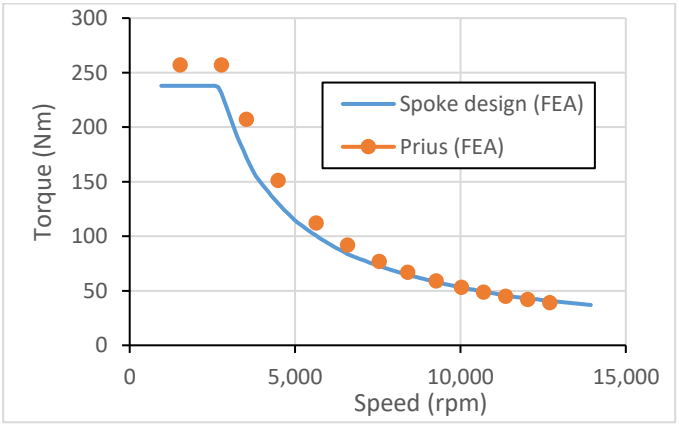

Fig. 11: Maximum torque vs. speed, new design compared to Prius 2010

This article has been accepted for publication in a future issue of this journal, but has not been fully edited. Content may change prior to final publication. Citation information: DOI 10.1109/TIA.2020.2966458, IEEE Transactions on Industry Applications

B. *Efficiency*

Fig. 12 captures the efficiency for the spoke design with 10% Nd, as calculated with MotorCAD software in the case where the rare-earth magnet is as long as the ferrite magnet (Fig. 4i and "Nd 1.0L" on Fig. 8). For comparison, Fig. 13 shows the efficiency for the baseline, also using MotorCAD software. These calculations include the copper and iron losses, but not the mechanical losses. The efficiency peak is over 97% for the new design. It is therefore slightly better than that at of the Prius 2010, which exceeds 96%, as illustrated in Fig. 13. The peak efficiency occurs around 4,000 rpm in both cases, and at slightly lower torque (ca. 40Nm) for the blended design compared to the baseline (ca. 60Nm).

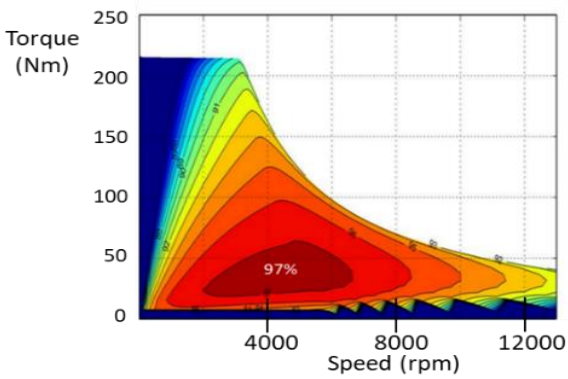

Fig. 12: Efficiency contours, spoke design, blended magnet

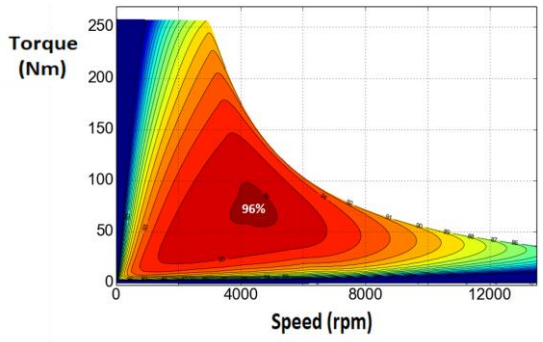

Fig. 13: Efficiency contours, baseline

C. *Mechanical analysis*

In order to estimate the structural integrity of the rotor, a mechanical analysis was conducted using the commercial ANSYS mechanical analysis software. The stress distribution at the maximum speed of 13,500 rpm (worst case mechanically speaking) was calculated using an assumption of slip between the magnets and laminations, which refers to allowing for relative motion between the two contact surfaces (also worst case mechanically speaking). The predicted Von Mises stress distribution for spoke type design is shown in Fig. 14. The peak stress point occurs at the contact surfaces between the rotor lamination and the hub. All the stress numbers are safely below 350 MPa (the yield strength of silicon steel laminations), which is considered the limit for lamination stacks. Note also that the magnet and hub dimensions where they meet could be easily adjusted to reduce the stress level (if need be) without impacting the magnetic performance significantly, as the portion of the magnet farthest from the airgap contributes the least magnetically.

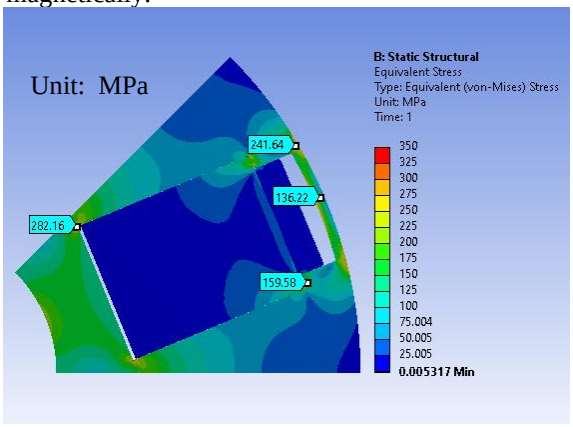

Fig. 14: Von Mises stress distribution at 13,500 rpm (with slip)

D. *Short-circuit analysis*

The analysis of the machine under short-circuit is of increasing interest to evaluate post-fault behavior, particularly so in the automotive industry where safety is a prime concern. It is well known that a full 3-phase short circuit is the least severe of all short circuits, and for this reason, many drives are designed to default to shorting all three phases in case any short circuit, partial or full, is detected. It is also a simple remedy, as it can be done through standard 3-phase inverters. This limits the short circuit current, and perhaps as importantly evens out the heat generated by the fault, avoiding potentially dangerous hot spots or sparks in the windings.

Accordingly, a study was conducted of 3-phase short circuits, via FEA. Fig. 15 shows results in the steady-state, short circuit current (Fig. 15a) and torque (Fig. 15b) versus speed. As seen in Fig. 15a, the steady-state short circuit current is at most 130A, which is smaller than rated current. The torque pattern is that of an induction machine torque with a synchronous speed of zero. The maximum torque occurs at very low speeds, as shown in the zoomed-in inset in Fig. 15b (-52Nm around 65rpm). The relatively low short-circuit current and torque, compared to maximum values, can perhaps be attributed to the relatively weak emf generated by the ferrite magnets, unlike the situation with all rare-earth magnet designs.

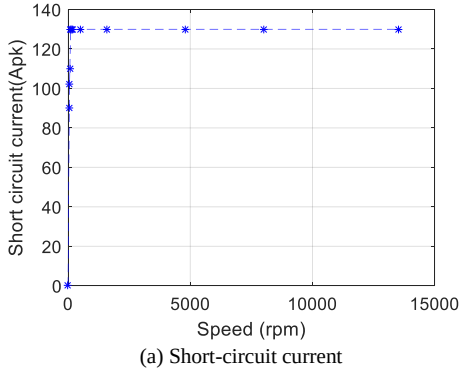

(a) Short-circuit current

This article has been accepted for publication in a future issue of this journal, but has not been fully edited. Content may change prior to final publication. Citation information: DOI 10.1109/TIA.2020.2966458, IEEE Transactions on Industry Applications

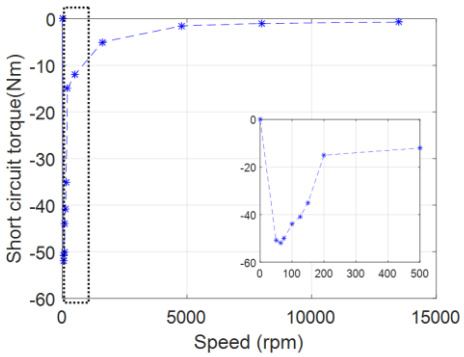

(b) Short-circuit torque (values at low speeds in figure inset)
Fig. 15: Steady-state short-circuit current and torque at 90°C

E. Demagnetization analysis

Demagnetization was assessed at three levels: First, with regular temperatures to study overcurrent behavior during short-circuits, then at extreme low and high temperatures. The calculations at regular temperature were performed with the machine at 60°C. The knee point B values (flux densities) are then -0.3T for NdFeB and -0.1T for ferrite.

A demagnetization coefficient is used for this analysis. It is defined as the difference between the knee point B value and the flux density in the direction of the magnetization, which means there is no demagnetization if the flux density in the direction of the magnetization is stronger than B at the knee point (if the demagnetization coefficient is negative). On the other hand, that magnet may be irreversibly demagnetized if the demagnetization coefficient is positive, that is if the flux density in the direction of magnetization is lower than the knee point.

Fig. 16 shows the demagnetization coefficients at 60°C under 2 times rated current and 1500 rpm operation condition. The value of 2 times rated current was used as an exemplary representation of transient currents during a short-circuit, before remedial action (such as shorting all 3 phases) is taken. A 40 degree current angle γ is assumed, corresponding to the value for maximum torque at lower speeds (as seen in Fig. 10). Fig. 16 (as well as subsequent, similar ones) focuses on one set of magnets (one pole), ferrite deeper in the rotor and rare-earth closer to the airgap. There is no risk of demagnetization under these conditions.

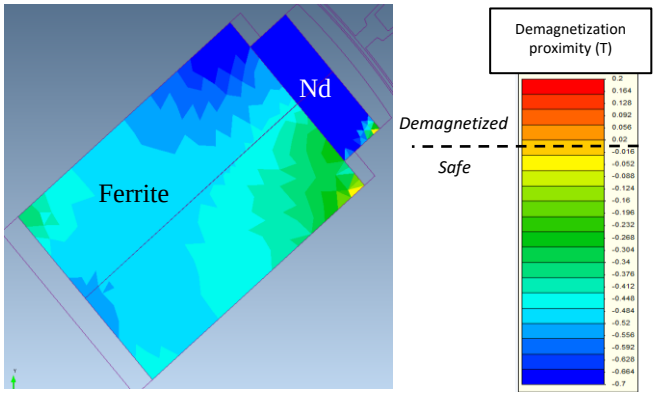

Fig. 16: Demagnetization proximity levels at 60°C, 500A/40 deg, 1500rpm

Demagnetization at temperature extremes must be performed at very low and very high levels, because of the magnets' different physical properties: Low temperature (-20°C) for ferrite and high temperature (up to at least 140°C) for Nd. The flux density (B) values at the knee points are 0.02T for ferrite at -20°C, and vary at high temperature depending on grade for NdFeB [19].

Turning first to low temperatures where ferrite is most at risk, Fig. 17 shows the demagnetization coefficients at -20°C under the 250A rated current and 1500 rpm operation condition. There is no risk of demagnetization (machine at -20°C) and maximum torque condition.

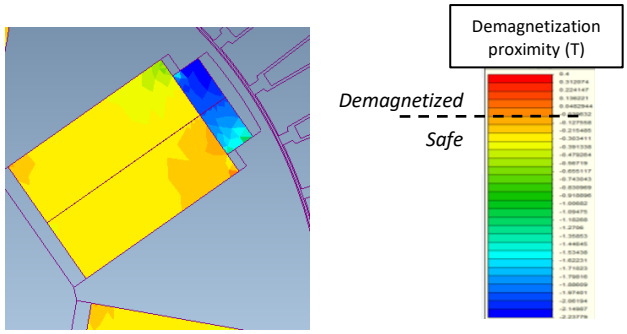

Fig. 17: Demagnetization proximity levels at -20°C, 250A/40 deg, 1500rpm

The study at higher temperature, where the focus is on the rare-earth magnets, was done by investigating current levels, control angle γ, temperature, and magnet grade.

Fig. 18 shows demagnetization for different current levels (rated and beyond, up to 2.5 times), γ=0, and two different magnet grades. The demagnetization proximity scale used in Fig. 18 is the same as the one in Fig. 17, where red colors indicate some level of demagnetization. The magnet grade on the left-hand side was N45SH [19], which has a B_r of 1.32T at room temperature, and a demagnetization knee value of 0.3T at 120°C. The plots on the right-hand side correspond to another magnet grade, N45UH [19], which has the same B_r of 1.32T at room temperature, but a lower demagnetization knee value of -0.1T at 120°C. While not specifically said in [19], it can be surmised that the UH grade has a higher heavy rare-earth (Dysprosium) content than the SH grade.

Concerning the N45SH rare-earth magnet, it is apparent that its corner closer to the airgap can demagnetize under these conditions. However, there is no demagnetization risk in the N45UH rare-earth magnet except in a very small portion in the corner, and only under 2.5 times rated current (Fig. 18e), which is a large safety margin. Importantly, and referring to Fig. 18b, right-hand side, at rated current, the flux density in the magnets is much higher than the value at the knee which would cover all normal operation as well as a 3-phase short circuit. These results indicate that blending of magnet types, like designs with rare-earth magnets only, need to carefully weigh magnet grade, but can operate safely under normal conditions, and with a full 3-phase short as a good remedy in case of a machine fault.

This article has been accepted for publication in a future issue of this journal, but has not been fully edited. Content may change prior to final publication. Citation information: DOI 10.1109/TIA.2020.2966458, IEEE Transactions on Industry Applications

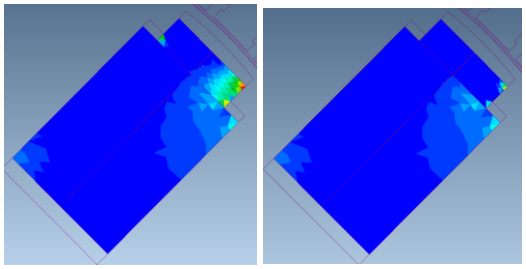

N45SH N45UH

(a) Magnets under 188A (75% of rated current)

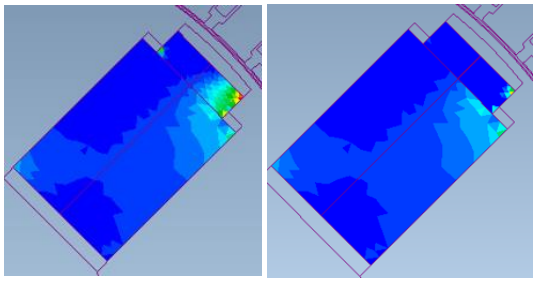

N45SH N45UH

(b) Magnets under 250A (rated current)

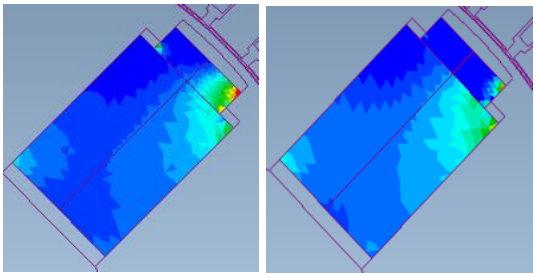

N45SH N45UH

(c) Magnets under 375A (1.5 times rated current)

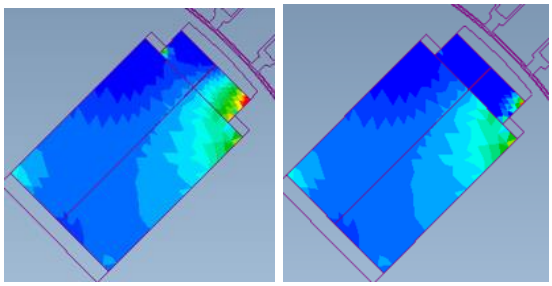

N45SH N45UH

(d) Magnets under 500A (2 times rated current)

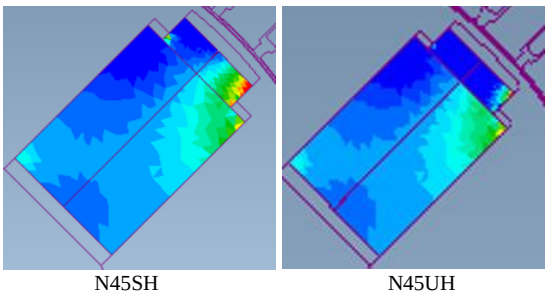

N45SH N45UH

(e) Magnets under 625A (2.5 times rated current)

Fig. 18: Demagnetization proximity levels under the rated current,1.5 times rated current, 2 times rated current and 2.5 times rated current at 120°C (γ =0, 1500 rpm)

Fig. 19 shows the demagnetization coefficients for various current angles with 2 times rated current at 120°C, all with a N45UH magnet (more resistant to demagnetization). The demagnetization proximity scale used in Fig. 19 is the same as before, where red indicates some level of demagnetization. As shown in the plot, there is no risk of demagnetization with 0 deg current angle. However, one end of the rare-earth magnet, again its corner closer to the airgap, can suffer demagnetization with current angles larger than 30 deg. But only a very small portion of one end of rare-earth magnet in the corner is affected, as illustrated in Fig. 19b, Fig. 19c and Fig. 19d. There is no demagnetization risk in most of the rare-earth magnet.

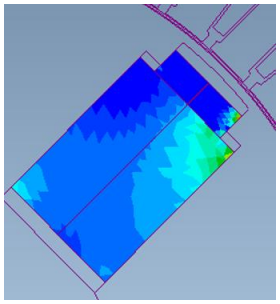

(a) Current angle γ =0 (500A)

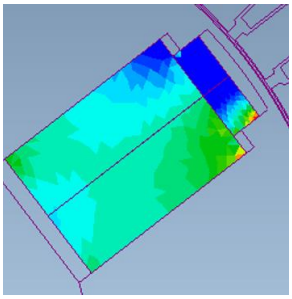

(b) Current angle γ =30 (500A)

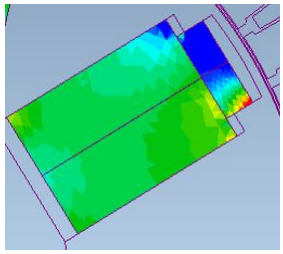

(c) Current angle γ =60 (500A)

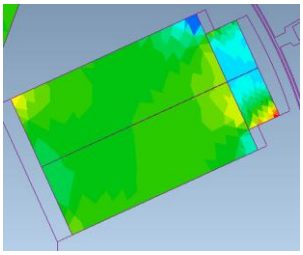

(d) Current angle γ =90 (500A)

Fig. 19: Demagnetization proximity levels for various current angles in N45UH under 2 times rated current at 120°C

Figs. 20 and 21 show the worse operating conditions in term of demagnetization. Fig. 21 shows the same two magnet grades at various higher temperatures (140°C, 130°C, 120°C and 110°C), and maximum rated current: N45SH on the left-hand side, and N45UH on the right-hand side. The N45SH magnet exhibits decreasing levels of demagnetization with temperature, with 110°C still being problematic, at least to a small degree. By contrast, the higher magnet grade (N45UH) can safely operate, even under peak current, up to approximately 130°C, at and above which temperature there may be some, but very limited and localized demagnetization. The problem is that the magnetic field deviates strongly from being parallel to magnetization near the airgap in the presence of a large opposing armature field. While the flux density overall in the magnet may still be reasonably high (say 0.6T or higher), the component in the direction of magnetization is too small to resist demagnetization.

This article has been accepted for publication in a future issue of this journal, but has not been fully edited. Content may change prior to final publication. Citation information: DOI 10.1109/TIA.2020.2966458, IEEE Transactions on Industry Applications

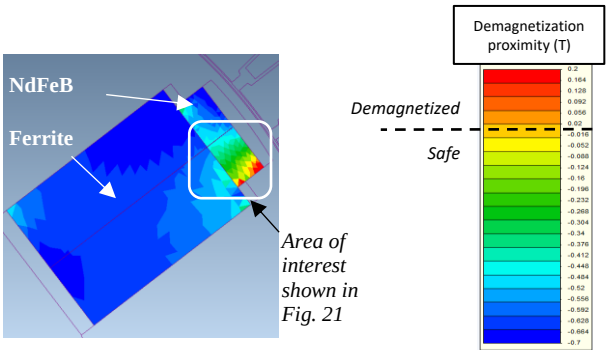

Fig. 20: Ferrite (bottom) and Nd (top) magnet demagnetization levels (left) and scale (right). Case shown: N45SH, 250A, γ =30°, 1500rpm, 140°C

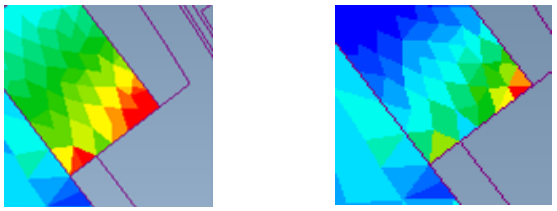

N45SH N45UH

(a) Nd magnet corner detail at 140ºC

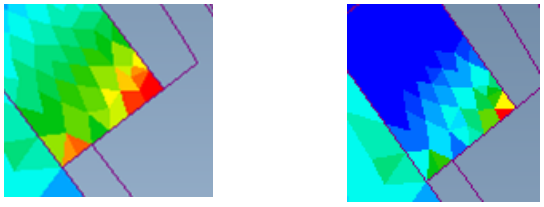

N45SH N45UH

(b) Nd magnet corner detail at 130ºC

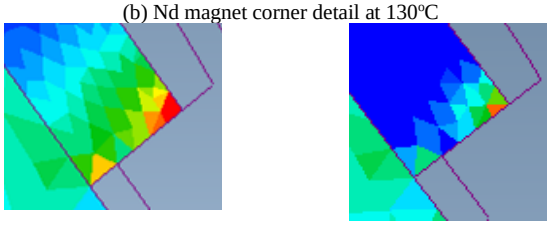

N45SH N45UH

(c) Nd magnet corner detail at 120ºC

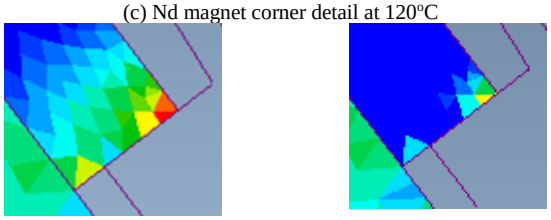

N45SH N45UH

(d) Nd magnet corner detail at 110ºC

Fig. 21: Demagnetization proximity levels in Nd magnet corner at peak current (250A, γ =30, 1500rpm) and elevated temperatures

Magnet grades with higher heavy rare-earth content are more expensive, but the cost may be acceptable as much less rare-earth magnet is used than in conventional IPM machines (some 60% less). The price assumed for the rare-earth magnet, $100/kg, can actually be considered to be on the high side, thus accommodating the more expensive additives. Just the same, it is clear that magnet demagnetization should be a focus of designs with multiple magnet types. Possible avenues include optimizing the magnet bridge, rare-earth magnet length and placement across the stator slots (which were unchanged from the Prius design), or still more performant magnet grades, such as N42EH, although these have lower remanent flux densities. Also, demagnetization analysis under more operating conditions especially under deep flux weakening needs to be performed.

F. Design consideration and optimization

The following presents an approach to improve the low-speed torque by appropriate shaping of the magnet, trading off magnet length for width, for instance.

For this purpose, a parameterized finite element model was developed, with the volume of the NdFeB magnet fixed at 10% that of the ferrite magnet. The key rotor design parameters are shown in Fig. 22. The model consists of six independent geometric variables in the rotor, with upper and lower boundaries to avoid geometric conflicts. During the optimization procedure, we only focused on a local optimization with single optimization objective of maximizing the torque performance. As mentioned earlier, this is an initial design and the stator configuration and airgap length are the same as for the baseline. The geometry of the ferrite and Nd magnets are considered as the main variables because they can have a large impact on the torque performance. The impact of the geometry of both ferrite and Nd magnets on the torque generation is illustrated in Fig. 23. The torque performance at each point in the Fig. 23 is calculated by FEA (MagNet).

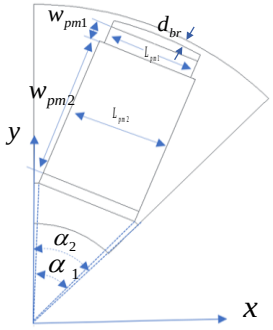

Fig. 22: Key rotor parameters for the proposed design

The ferrite magnet width w_{pm2} and length L_{pm2} have to be large enough to produce sufficient torque. However, the amount of ferrite is limited by the available space in the rotor, specifically by the chord length where the magnet is deepest in the rotor. Fig. 23 shows the impact of Nd length L_{pm1} and ferrite length L_{pm2} on the torque production with 10% Nd magnet. Torque is significantly dependent on the magnet length. Torque output gradually increases as the ferrite length L_{pm2} increases, until it reaches a limit due to the chord length for this rotor diameter and number of poles. Concerning the Nd length L_{pm1}, an optimum is reached that is shorter than ferrite magnet length. The optimum corresponds to the longest possible ferrite magnet (26mm) and a shorter, 16.3mm long Nd magnet. The key parameters of the resulting design are given in Table II.

This article has been accepted for publication in a future issue of this journal, but has not been fully edited. Content may change prior to final publication. Citation information: DOI 10.1109/TIA.2020.2966458, IEEE Transactions on Industry Applications

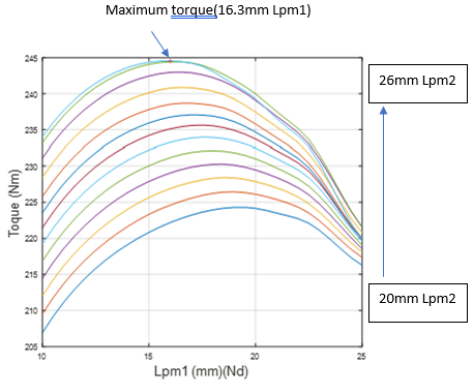

Fig. 23: Torque for various magnet lengths, spoke type with 10% NdFeB

TABLE II
KEY ROTOR PARAMETERS FOR PROPOSED DESIGN

Dimensions(mm)	Proposed design
Nd length L_{pm1}	16.3
Nd width w_{pm1}	6.1
Ferrite length L_{pm2}	26
Ferrite width w_{pm2}	33.9
Bridge depth d_{br}	0.67

IV. CONCLUSION

In order to reduce the cost of high-performance IPM machines, the paper proposes different rotor configurations with a blend of ferrite and rare-earth magnets. Performance is compared to a baseline production design with conventional Nd-based magnets (Prius 2010). The results show that a blended-magnet spoke design with unequal magnet lengths can generate a comparable torque to the baseline design with ~ 60% reduction in rare-earth PM volume, and lower overall cost. In terms of the comparison of torque per dollar, the spoke type with unequal magnet lengths has an advantage over other topologies, which means the proposed spoke type IPM design can be a potential candidate for reducing IPM cost with no loss in performance.

Ref. 16 showed, perhaps for the first time, that an IPM machine designed with a blend of ferrite and rare-earth magnets could achieve the same performance as a machine with rare-earth magnets only. The design in [16] was V shape. In this paper, a more systematic analysis of various rotor topologies was conducted, and the conclusion is that spoke-type configurations may have even better potential in this regard, due to a strong "funnel" effect for the magnetic flux, such that the relatively weak flux density from the ferrite magnets is amplified to a level comparable to that of conventional, V-patterned, rare-earth IPMs, that is, to the point of steel saturation.

ACKNOWLEDGMENT

The authors are grateful to Mr. Rasul Hemmati for contributing the mechanical analysis and Mr. Yue Sun for some of the efficiency analysis using Motor CAD.

REFERENCES

[1] S.M. Jang, et. al., "Design and electromagnetic field characteristic analysis of 1.5 kW small scale wind power generator for substitution of Nd-Fe-B to ferrite permanent magnet," IEEE Trans. on Magn., Vol. 48, No. 11, Nov. 2012, pp. 2933-2936.

[2] M. Barcaro and N. Bianchi, "Interior PM machines using ferrite to replace rare-earth surface PM machines," IEEE Trans. on Indus. Appl., Vol. 50, No. 2, March/April 2014, pp. 979–985.

[3] J. McFarland, T. Jahns, A. EL-Refaie and P. Reddy, "Effect of magnet properties on power density and flux-weakening performance of high-speed interior permanent magnet synchronous machines," in Proc. of the 2014 ECCE Conf., Pittsburgh, PA, USA, Sept. 14–18, pp. 4218–4225.

[4] S.J. Galioto, P.B. Reddy, A.M. EL-Refaie and J.P. Alexander, "Effect of magnet types on performance of high-speed spoke interior-permanent-magnet machines designed for traction applications," IEEE Trans. on Indus. Appl., Vol. 51, No. 3, May/June 2015, pp. 2148-2160.

[5] S. Jurkovic, K. Rahman, B. Bae, N. Patel and P. Savagian, "Next generation Chevy Volt electric machines; design, optimization and control for performance and rare-earth mitigation," in Proc. of the 2015 IEEE ECCE, Montreal, QC, Canada, Sept. 20-24, pp. 5219-5226.

[6] M. Kimiabeigi, et. al., "High-performance low-cost electric motor for electric vehicles using ferrite magnets," IEEE Trans. on Indus. Electronics, Vol. 63, No, 1, Jan. 2016, pp. 113-122.

[7] C.-L Jeong and J. Hur, "A novel proposal to improve reliability of spoke-type BLDC motors using ferrite permanent magnet", IEEE Trans. on Indus. Appl., Vol. 52, No. 5, Sept./Oct. 2016, pp. 3814-3821.

[8] A. EL-Refaie, et. al., "Comparison of traction motors that reduce or eliminate rare-earth materials," IET Electrical Systems in Transportation, Vol. 7, No. 3, Sept. 2017, pp. 207-214.

[9] A. Fatemi, et. al., "Design of an electric machine for a 48-V mild hybrid vehicle," in Proc. of the 2018 IEEE ECCE Conf., Portland, OR, USA, pp. 2278-2285.

[10] Z.S. Du and T.A. Lipo, "Torque performance comparison between a ferrite magnet Vernier motor and an industrial interior permanent magnet machine," IEEE Trans. on Indus. Appl., Vol. 53, No. 3, May/June 2017, pp. 2088-2097.

[11] S. Li, Y. Li and B. Sarlioglu, "Partial irreversible demagnetization assessment of flux-switching permanent magnet machine using ferrite permanent magnet material," IEEE Trans. on Magn., Vol. 51, No. 7, July 2015.

[12] J.D. McFarland, T.M. Jahns and A.M. EL-Refaie, "Performance and efficiency comparisons for interior PM and flux-switching PM machines with ferrite magnets for automotive traction applications," in Proc. of the 2015 IEEE ECCE, Montreal, QC, Canada, Sept. 20-24, pp. 6529-6536.

[13] H. Hua, Z.Q. Zhu, C. Wang, M. Zheng, Z. Wu, D. Wu and X. Ge, "Partitioned stator machines with NdFeB and ferrite magnets," IEEE Trans. on Indus. Appl., Vol. 53, No. 3, May/June 2017, pp. 1870-1882.

[14] T. Masuko and I. Miki, "A novel rotor structure of IPMSM with rare earth and ferrite magnets," in Proc. of the 2016 International Conference on Electrical Machines and Systems, Chiba, Japan, pp. 1-5.

[15] C.-L. Jeong, Y.-K. Kim and J. Hur, "Optimized design of PMSM with hybrid-type permanent magnet for improving performance and reliability," IEEE Trans. on Indus. Appl., Vol. 55, No. 5, Sept./Oct. 2019, pp. 4692-4701.

[16] Z.S. Du and T.A. Lipo, "Interior permanent magnet machines with rare earth and ferrite permanent magnets", in Proc. of the 2017 IEEE International Electric Machines & Drives Conference (IEMDC), Miami, FL, USA, May 21-24.

[17] Q. Ma, A. EL-Refaie and B. Lequesne, "Low-cost interior permanent magnet machine with a blend of magnet types" in Proc. of the 2019 IEEE International Electric Machines & Drives Conference (IEMDC), San Diego, CA, USA, May 12-15, pp. 1303-1310.

[18] T.A. Burress, et. al., "Evaluation of the 2010 Toyota Prius hybrid synergy drive system," ORNL report to DOE, ORNL/TM-2010-253, Mar. 2011.

[19] Anon., "Neodymium-iron-boron magnet grades", Arnold Magnetic Technologies catalog, Rev. 181031. Available at: https://www.arnoldmagnetics.com/wp-content/uploads/2017/10/Catalog-151021.pdf (retrieved March 31, 2019)

[20] J. Gambogi, USGS, "Rare earths". Available at: https://minerals.usgs.gov/minerals/pubs/commodity/rare_earths/mcs-2019-raree.pdf (retrieved March 21, 2019).

[21] M. Burwell, J. Goss and M. Popescu, "Performance/cost comparison of induction motor and permanent-magnet-motor in a hybrid electric car", July 2013. Available at: www.coppermotor.com/wp-content/uploads/2013/08/Techno-Frontier-2013-MBurwell-ICA-EV-Traction-Motor-Comparison-v1.8-Eng1.pdf (retrieved Dec. 20, 2017).